RESEARCH ARTICLE

Development of a mouse model of chronic ventral spinal cord compression: Neurobehavioral, radiological, and pathological changes

Zhongyuan He[1,2] (iD) | Tao Tang[1,3] | Zhengya Zhu[1,4] | Fuan Wang[1] |
Jianfeng Li[1] | Fu Zhang[1] | Nguyen Tran Canh Tung[5] | Shaoyu Liu[6] |
Xizhe Liu[6] | Zhiyu Zhou[1] (iD)

[1]Innovation Platform of Regeneration and Repair of Spinal Cord and Nerve Injury, Department of Orthopedic Surgery, The Seventh Affiliated Hospital of Sun Yat-sen University, Shenzhen, China

[2]Department of Orthopedics, The Second Affiliated Hospital of Chongqing Medical University, Chongqing, China

[3]Department of Orthopedics, The Second Affiliated Hospital of Anhui Medical University, Hefei, China

[4]Department of Orthopedics, Affiliated Hospital of Xuzhou Medical University, Xuzhou, China

[5]Department of Orthopedic Surgery, Faculty of Medicine, University of Toyama, Toyama, Japan

[6]Guangdong Provincial Key Laboratory of Orthopedics and Traumatology, The First Affiliated Hospital of Sun Yat-sen University, Guangzhou, China

Correspondence
Xizhe Liu, The First Affiliated Hospital of Sun Yat-sen University, Guangzhou 510080, China.
Email: liuxizhe@mail.sysu.edu.cn

Zhiyu Zhou, The Seventh Affiliated Hospital of Sun Yat-sen University, Shenzhen 518107, China.
Email: zhouzhy23@mail.sysu.edu.cn

Funding information
Sanming Project of Medicine in Shenzen Municipality, Grant/Award Number: SZSM201911002; National Natural Science Foundation of China, Grant/Award Numbers: U22A20162, 31900583, 32071351, 81772400, 82102604, 81960395; the Natural Science Foundation of Guangzhou City, Grant/Award Number: 201807010031; the Beijing Municipal Health Commission, Grant/Award Numbers: BMHC-2021-6, BMHC-2019-9, BMHC-2018-4; AOCMF Translational approaches for bone constructs, Grant/Award Number: AOCMF-21-04S; Foundation of Shenzhen Committee for Science and Technology Innovation, Grant/Award Numbers: JCYJ20190809142211354, GJHZ2018 0929160004704; Academic Affairs Office of

Abstract

Objectives: The main objective of this study was to establish a mouse model of spinal ligament ossification to simulate the chronic spinal cord compression observed in patients with ossification of the posterior longitudinal ligament (OPLL). The study also aimed to examine the mice's neurobiological, radiological, and pathological changes.

Methods: In the previous study, a genetically modified mouse strain was created using Crispr-Cas9 technology, namely, $Enpp1^{flox/flox}$/*EIIa-Cre* (C57/B6 background), to establish the OPLL model. Wild-type (WT) mice without compression were used as controls. Functional deficits were evaluated through motor score assessment, inclined plate testing, and gait analysis. The extent of compression was determined using CT imaging. Hematoxylin and eosin staining, luxol fast blue staining, TUNEL assay, immunofluorescence staining, qPCR, and Western blotting were performed to evaluate levels of apoptosis, inflammation, vascularization, and demyelination in the study.

Results: The results demonstrated a gradual deterioration of compression in the $Enpp1^{flox/flox}$/*EIIa-Cre* mice group as they aged. The progression rate was more rapid between 12 and 20 weeks, followed by a gradual stabilization between 20 and 28 weeks. The scores for spinal cord function and strength, assessed using the Basso Mouse Scale and inclined plate test, showed a significant decline. Gait analysis revealed a noticeable reduction in fore and hind stride lengths, stride width, and toe

spread. Chronic spinal cord compression resulted in neuronal damage and activated astrocytes and microglia in the gray matter and anterior horn. Progressive posterior cervical compression impeded blood supply, leading to inflammation and Fas-mediated neuronal apoptosis. The activation of Bcl2 and Caspase 3 was associated with the development of progressive neurological deficits ($p < 0.05$).

Conclusions: The study presents a validated model of chronic spinal cord compression, enabling researchers to explore clinically relevant therapeutic approaches for OPLL.

KEYWORDS

apoptosis, chronic spinal cord injury, motor function, myelopathy, OPLL, pathophysiological changes

1 | INTRODUCTION

Ossification of the posterior longitudinal ligament (OPLL) is a prevalent degenerative disease characterized by progressive ossification. Without timely and effective treatment, the compression of the spinal cord by ossified tissue can result in chronic spinal cord injury and subsequent limb paralysis. At present, there is no effective treatment other than surgery for OPLL.[1–3] Mechanical compression of the spinal cord can lead to reduced activity in neuronal cells, demyelination of axons, damage to nerve tissue, decreased protein synthesis, and even neuronal death.[4–6] Nevertheless, the mechanisms responsible for these pathological changes remain unclear, partly because it is difficult to estimate the changes in human and animal experiments, as well as the scarcity of suitable animal models for studying long-term compression-induced progressive spinal cord injury.[7]

Previous studies have employed various animal models to simulate chronic spinal cord compression, such as tumor cells, screws, dilated sacs, and hydrophilic polymers.[8–11] During the initial stages of spinal cord compression research, tumor cell transplantation emerged as a frequently employed technique. Additionally, the gradual tightening of screws, including titanium screws and root canal screws, was utilized to induce spinal cord compression. An alternative technique for inducing spinal cord compression involves the insertion of a dilatation balloon into the epidural or subarachnoid space using a catheter. In recent years, hydrophilic swelling polymers have gained traction as a means to replicate progressive spinal cord compression.[12] Researchers have recently used the tip-toe Walking Yoshimura (twy/twy) mouse, a unique animal that presents with spontaneous spinal cord compression, providing a good in vivo model of chronic cervical spondylosis. The twy mice develop progressive spinal cord dysfunction secondary to C2-3 epidural calcific deposits, leading to compression of the cervical spinal cord. OPLL-induced neuropathies in twy/twy mice, including paralysis and spasticity, are similar to those observed in humans, and OPLL-induced chronic spinal cord injury is simulated.[13] However, obtaining twy mice is challenging and may have limited availability. Multiple incisions and sutures cause wound infection and increase mortality, and tumor models may have irregular

shapes, resulting in varying degrees of compression and poor reproducibility. Most of the spinal cord compressions in the models are short-term and do not adequately simulate the situation in which cervical spondylotic myelopathy (CSM) or OPLL results in chronic spinal cord compressions.[14,15] Spinal cord compression in animal models primarily occurs dorsally, whereas in cases of OPLL, the compression predominantly affects the ventral side.

Based on our previous studies, we developed *Enpp1*[flox/flox]*/EIIa-Cre* mice, which were obtained by crossing Enpp1[CKI/+] mice created using gene editing technology with EIIa-Cre tool mice. The mice exhibited ectopic ossification of spinal ligaments within the spinal canal, leading to chronic compression of the ventral spinal cord. This study aimed to develop a reliable model of chronic spinal cord injury, allowing for the identification of potential therapeutic interventions to enhance spinal cord function in individuals with OPLL.

2 | MATERIALS AND METHODS

2.1 | Animals and diet

By employing CRISPR-Cas9 technology, we successfully introduced a stop codon at position 568 in the Enpp1 gene, generating *Enpp1*[flox/flox]*/EIIa-Cre* mice (Figure S1A). The Enpp1 gene produces diphosphate (ppi) and a nucleotide pyrophosphatase, which are important for bone mineralization and soft tissue calcification by regulating pyrophosphate levels, while ppi inhibits bone mineralization and soft tissue calcification by binding to nascent hydroxyapatite crystals, preventing further growth of these crystals. The loss of Enpp1 expression results in ectopic ossification of the spine. EIIa-Cre mice carry a Cre transgene under the control of the adenoviral EIIa promoter, which targets the expression of Cre recombinase to the early mouse embryo and is useful for the deletion of loxP-flanked genes in the germline. Cre-mediated recombination occurs in a wide range of tissues, including the germ cells that transmit the genetic alteration to progeny. In general, there were 48 mice in the three groups of *Enpp1*[flox/flox]*/EIIa-Cre* (12, 20, and 28 weeks) and WT group (28 weeks), and 12 mice were

needed in each group. For each group, six tissues requiring paraformaldehyde perfusion after sacrifice (4 were randomly selected for CT scanning) were further histologically verified. RNA and protein of the spinal cord were extracted from the remaining six mice in fresh tissue samples and perfused with frozen PBS for the RT-qPCR and WB analysis. Among them, nine *Enpp1* flox/flox/*EIIa-Cre* and nine WT mice, all of the same age, were subjected to behavioral observation during 28 weeks of feeding.

Our previous studies have confirmed that *Enpp1*flox/flox/*EIIa-Cre* mice exhibit ectopic spine ossification. For the experiments conducted, only male mice were utilized due to the need to breed enough female mice to obtain the desired genotypes. Mice were weaned at 3–4 weeks of age and kept on a standard laboratory diet. Behavioral experiments were conducted under a 12-h light and 12-h dark cycle. In this study, we utilized *Enpp1*flox/flox/*EIIa-Cre* mice (each group, $n = 12$) and WT mice ($n = 12$) as control groups based on previous study and published literature.[16] All experimental procedures were approved by the Institutional Animal Care and Use Committee of Sun Yat-Sen University (No. 2020000147).

2.2 | Neurobehavioral testing

The flowchart is shown in Figure 1A. At 12, 20, and 28 weeks, we examined locomotor function in *Enpp1*flox/flox/*EIIa-Cre* mice and WT mice. In this study, the Basso Mouse Scale (BMS) scoring tools were used (Table S1). An assessment was conducted by trained, blinded investigators, and a consistency score was calculated. The BMS is a sensitive, valid, and reliable tool for measuring motor function in mice with spinal cord injuries. Depending on the position of the mouse's paws and the instability of its trunk, a 10-point scale (0–9 points) was used to assess the degree of instability, supplemented with a BMS scoring form as detailed in Table S1.[17] In general, a score of 9 indicates normal movement and a score of 0 indicates complete paralysis of the hindlimbs.

2.3 | Assessment of locomotor function

Inclined plane test: Animals were placed individually on a 28×30 cm plate covered with a grooved rubber surface, and their ability to maintain body position was evaluated as the plates were gradually raised to increasing angles. As the tilt angle increased toward the vertical position, the animal could no longer maintain stability. We assigned a score based on the maximum angle of inclination at which an animal was able to maintain a stable body position for 5 s.

Footprint analysis: A walking track footprint analysis was conducted using the method described by de Medinaceli et al. with modifications.[18] In both the front and hind paws of the animals, nontoxic dyes were applied. As the mice walked from a brightly lit start frame to a dark box with food baits at the end of the box, they passed through a narrow wooden board measuring approximately 0.5 m in length and 10 cm in width. The footprints were scanned and digitized by measuring the images. Toe extension was measured as the distance between the first and fifth toes of the forepaw, and interarm coordination was measured as the distance between the ipsilateral forepaw (pad center) and hindpaw (pad center). Three mice from each group underwent BMS and inclined plane tests at 12, 20, and 28 weeks, while another set of nine from each group underwent footprint analysis at the same time points.

2.4 | Micro-CT analyses

Micro-CT analysis (SCANCO MEDICAL, μCT100 Bassersdorf) was performed, scan energy intensity 70 KVP, 200 μA; filter tablet 0.5 Al; CT values corrected to 1200 mgHA/cm; image matrix 3072×3072; FOV 75 mm, resolution 24.5 μm. Sampletim (exposure time) 300 ms. Software, including CTVol v.2.2.1, CTAn v.1.18.4.0 (Bruker, Kontich, Belgium), and ImageJ v1.53e (Media Cybernetics, Inc., Rockville, MD), was used to analyze the reconstructed images. For CT evaluations, each mouse had its minimum diameter measured four times on different sections near the sagittal axis at approximately the mid-horizontal position. Concurrently, the transverse sections of the cervical spine were horizontally divided into four equal segments, with the measurement of the minimal area conducted and recorded for subsequent statistical analysis.

2.5 | Tissue processing

To determine the degree of spinal canal compression and heterotopic ossification of the spine in mice, we sacrificed the mice by deep anesthesia after completing all the observation trials, and the scanning was performed after formaldehyde systemic perfusion to fix the tissue samples. Sacrificed *Enpp1*flox/flox/*EIIa-Cre* mice starting at 12 weeks of age and subsequently every 8 weeks until reaching 28 weeks of age, While the WT group collected data at the corresponding time points and sacrificed at 28 weeks. The animals were administered an overdose of isoflurane inhalant.

For tissue preparation, transcardial perfusion and fixed with 4% paraformaldehyde (PFA, Biosharp) overnight. After washing with PBS (Solarbio) for three times (20 min each). Then decalcify with 12.5% EDTA decalcification solution (Leagene Biotechnology) for 1–2 weeks, with a solution change every 2 days until decalcification was complete. After washing with PBS buffer, specimens were incubated in PBS solution containing 30% (w/v) sucrose (Biofroxx) for 24 h. We used standard sectioning techniques, ensuring that for sagittal sections, the cut was made in the central position of the spine to obtain a comprehensive view of the anatomy. The sampling of axial sections was based on the CT evaluation of the characteristics of the vertebral body, Both *Enpp1*flox/flox/*EIIa-Cre* and WT mice at 28 weeks were selected for histological sections. Because *Enpp1*flox/flox/*EIIa-Cre* mice were found to be most severely compressed at T1 level, the
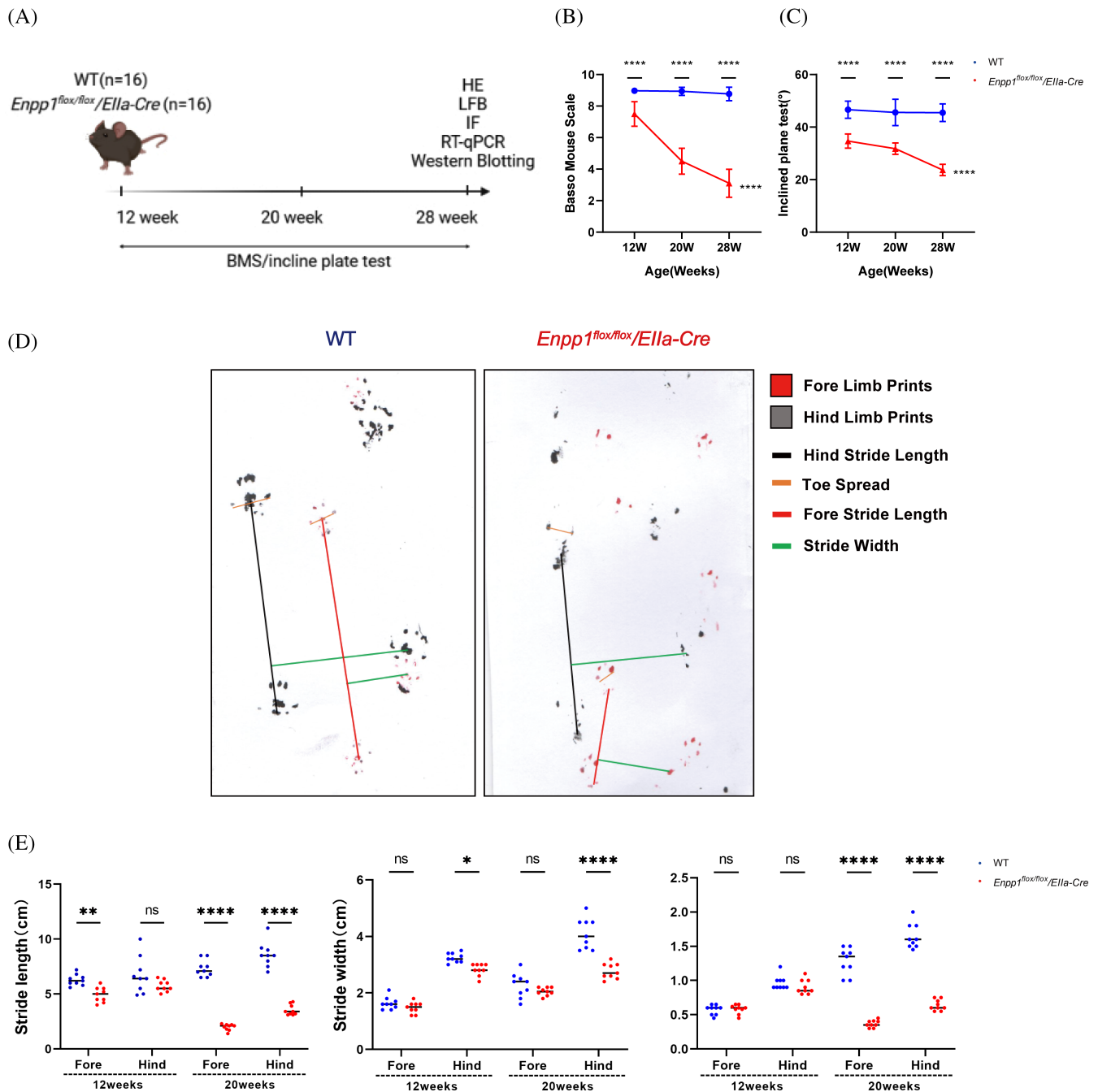
FIGURE 1 Functional assessment reveals impaired motor in *Enpp1flox/flox/EIIa-Cre* mice compared to the WT group. Behavioral tests were performed on the same group of mice (9 *Enpp1flox/flox/EIIa-Cre* and 9 WT) over different time points. (A) Experimental design. (B) Walking ability as determined by BMS scores. Hindlimb function was scored from 0 to 9 (flaccid paralysis to normal gait). (C) Animals were tested using the inclined plane test, and the angle (°) was recorded to reveal motor function recovery for week 12, week 20, and week 28. (D) Raw data from animals on the walkway in real color. (E) The step length and step width of *Enpp1flox/flox/EIIa-Cre* mice were significantly unbalanced, and the Toe spread was significantly reduced compared with WT. Differences were greater at 20 weeks. Data are expressed as mean ± SD. *$p < 0.05$, **$p < 0.01$, ***$p < 0.001$, ****$p < 0.0001$, *Enpp1flox/flox/EIIa-Cre* versus WT group.

corresponding segments were also selected for wt to ensure consistency of comparison. We performed a systematic analysis of all slices to ensure that our findings were reliable and reproducible. Finally, the specimens were embedded in the optimum cutting temperature (O.C.T, SAKURA) compound, and frozen sections were then sliced to a thickness of 10 mm.

2.6 | RNA extraction and quantitative real-time polymerase chain reaction (qRT–PCR)

After receiving an overdose of inhaled isoflurane, the animals were prepared for transcardial perfusion with phosphate-buffered saline (PBS, pH 7.4) followed by spinal cord dissection. We obtained fresh samples

from the cervical and thoracic segments of the spinal cord for dissection, which we used to isolate tissue and extract RNA at the most severely compressed part. The RNeasy Animal RNA Extraction Kit (Beyotime) was used for RNA extraction. Spinal cord tissue was rapidly minced on ice and lysed, and cDNA was synthesized using the Primescript RT Master Mix (perfect real-time) cDNA Synthesis Kit (Takara Biomedical Technology, Beijing, CHN). PowerUp SYBR Green Master Mix (Thermo Fisher Scientific, USA) was used for qRT–PCR (Bio-Rad). Each reaction mixture was 10 μl and contained 2 μl of 5 ng/μl cDNA, 5 μl of 2× PowerUp SYBR Green Master Mix, 2 μl of nuclease-free water, and 0.5 μl each of 10 μM forward and reverse primers. The following thermocycler conditions were used: 50°C for 2 min; 95°C for 2 min; and 44 cycles of 15 s at 95°C and 1 min at 60°C. The specific primers used in this study were designed using Primer 6.0 software (Applied Biosystems) (Table S2). The data were analyzed using the $2^{-\Delta\Delta Ct}$ algorithm.

2.7 | Efficient protein extraction methods for western blot analysis

For spinal cord protein analysis, the principle of selecting tissue sites is consistent with the method in Section 2.6. Place the dounce grinder on ice that has been pre-cooled, wash the spinal cord three times with cold PBS, and then shred it before placing it in the desired location. In the presence of 1% HaltTM protease inhibitor cocktail (Thermo Fisher Scientific) and 1% PMSF (Boster), the tissues were lysed using RIPA lysis buffer (Boster and subjected to 30 s of ultrasound treatment; Sonics CVX130). After centrifugation at 12000*g* at 4°C for 10 min, the protein was separated. The protein extract was resolved using NuPAGE 4%–12% Bis-Tris gel (Invitrogen), and subsequently transferred onto a PVDF membrane (Invitrogen) through electroblotting. Following a water rinse, the membrane was sealed at room temperature with 5% skimmed milk powder in TBST (Biosharp) under continuous stirring for 1 h. Subsequent to membrane sealing, the PVDF membrane was incubated with the following primary antibodies, appropriately diluted in TBST, at 4°C: anti-ARG1 (1:1000, AF1381, Beyotime), anti-MRC1 (1:1000, AF7500, Beyotime), anti-NeuN (1:1000, GB11138, Servicebio), anti-cleaved CASP3 (1:5000, ab214430, Abcam), anti-VEGF (1:1000, AF1309, Beyotime), and anti-GAPDH (1:1000, D16H11, Cell Signaling Technology). Subsequently, the membrane was subjected to three washes with TBST.

Next, the membrane was exposed to a secondary antibody, goat anti-rabbit HRP (1:4000, ab205718, Abcam), at room temperature for 1 h. After incubation, the membrane was washed three times with TBST to eliminate any unbound antibodies. Immunoblotting signals were visualized using an ECL reagent (Beyotime). The entire experimental procedure was repeated three times to ensure the reproducibility of the results.

2.8 | Histological analysis and immunohistochemical analysis

Hematoxylin–eosin (HE) staining (C0105S, Beyotim) and luxol fast blue (LFB) staining (RS1730, Gclone) were performed according to standard protocols. Images were captured using the Leica DM4B system and the Digital Pathology Section Scanner (KF-PRO-005, KFBIO technology). For immunofluorescent staining, samples were incubated with an antibody against IBA1 (GB113502, Servicebio). For immunohistochemical visualization of the astrogliosis and protoplasmic astrocytes, samples were incubated with anti-GFAP (GB11096, Servicebio), anti-NeuN (GB11138, Servicebio), anti-von willebrand factor (GB11020, Servicebio), Anti-Myelin Basic Protein (GB11226, Servicebio), anti-Fas ligand (GB11090, Servicebio), and anti-VEGF (Beyotime, AF1309) antibodies overnight at 4°C followed by incubation with a donkey anti-rabbit IgG (H + L) Highly Cross-Adsorbed Secondary Antibody, Alexa Fluor Plus 488 (A11008, Thermo Fisher Scientific) and donkey anti-rabbit IgG (H + L) Highly Cross-Adsorbed Secondary Antibody, Alexa Fluor Plus 594 (A32754, Thermo Fisher Scientific) secondary antibodies for 1 h. Subsequently, the samples were stained with DAPI. Images were captured with a Leica DM6B system microscope. The intensity of each fluorescence intensity signal obtained was evaluated by ImageJ software (NIH, Bethesda, MD).

2.9 | Statistical analysis

Quantification was performed from at least three independent experimental groups and presented as the mean ± SD. Statistical analysis was performed using GraphPad Prism 9 software (GraphPad Software Inc., San Diego, CA). For quantitative data, Shapiro–Wilk (S–W) is used to test whether the data conform to normal distribution and to test the hypothesis of homogeneity of variance. If the data conforms to the normal distribution and the homogeneity test of variance, the t-test is used for the comparison between two groups, and one-way ANOVA is used for the comparison between multiple groups. If there were significant differences in the results of one-way ANOVA, the Bonferroni test was used for multiple comparisons. For behavioral observation, we used two-way ANOVA for statistical analysis. Significance was indicated by asterisks (*$p < 0.05$, **$p < 0.01$, ***$p < 0.001$, and ****$p < 0.0001$), and $p < 0.05$ was considered significant.

3 | RESULTS

3.1 | Age-related decline in motor ability and impaired limb strength in mice

We selected mice at 12, 20, and 28 weeks of age based on previous findings indicating the onset of walking dysfunction in the test group at 12 weeks. Additionally, behavioral differences between 20 and 28 weeks were relatively minimal. The BMS score and inclined plane test were used to record motor function. Compared to the WT group, the *Enpp1^flox/flox^/EIIa-Cre* group showed a significant reduction in the BMS score at 12 weeks (7.29 ± 0.77), 20 weeks (4.13 ± 0.88), and 28 weeks (3.00 ± 0.84) (Figure 1B). At the same time, the inclined plane test showed that the *Enpp1^flox/flox^/EIIa-Cre* group had a smaller angle and could maintain 34.46 ± 2.36° at 12 weeks but only 24.21
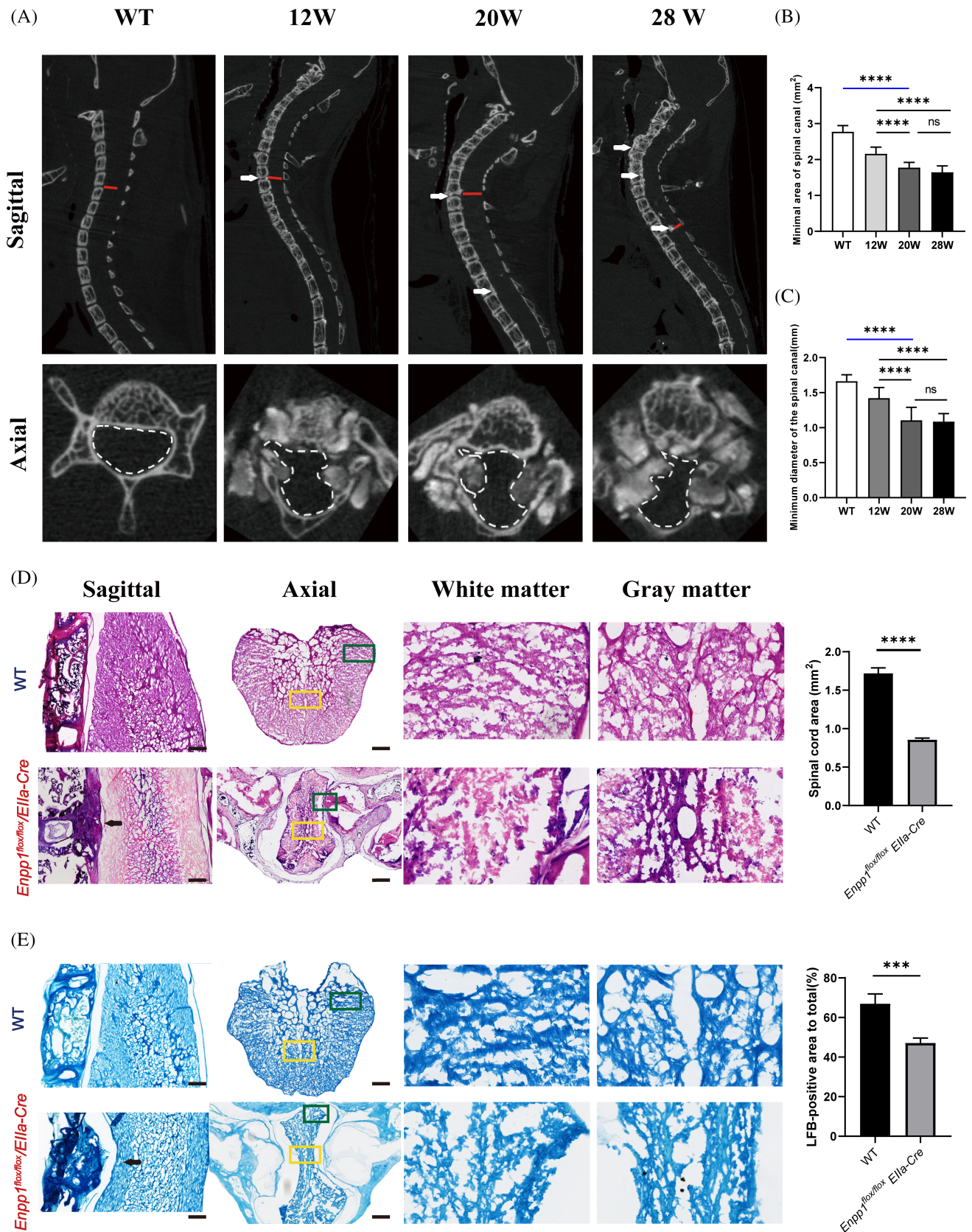
(A)

| | WT | 12W | 20W | 28 W |

(B)

(C)

(D)

| | Sagittal | Axial | White matter | Gray matter |

(E)

FIGURE 2 Legend on next page.

± 2.35° at 28 weeks (Figure 1C). In general, The *Enpp1flox/flox*/*EIIa-Cre* group showed significantly reduced mobility compared to the WT group.

3.2 | Basal broad-based spastic gait pattern in *Enpp1flox/flox*/*EIIa-Cre* mice

As demonstrated in Figure 1D, WT mice displayed a balanced 1:1 ratio of fore- to hindlimb steps, along with overlapping fore- and hindlimb placements. In the case of *Enpp1flox/flox*/*EIIa-Cre* mice, we observed a notable disparity in step length and stride width between the left and right feet. Additionally, the mice exhibited smaller toe spread, indicating an imbalance. These findings suggest a significant reduction in physiological function for mice with spinal cord compression. The *Enpp1flox/flox*/*EIIa-Cre* group between 12 and 20 weeks of age exhibited the most rapid progression of gait abnormalities. Gait analysis demonstrated a significant reduction in fore stride length, fore stride width, fore toe spread, hind stride length, hind stride width, and hind toe spread in the *Enpp1flox/flox*/*EIIa-Cre* group compared to the WT group. Moreover, as the mice aged, the disparity between the two groups became more pronounced, indicating a worsening of the gait abnormalities (Figure 1E).

3.3 | CT radiological observations

Sagittal and axial CT imaging of the cervical spine was employed to assess the location and severity of cervical spinal cord compression. The results showed that the mice in the WT group had no spinal stenosis, while spinal stenosis in the *Enpp1flox/flox*/*EIIa-Cre* group occurred in multiple segments not only from the anterior compression but also from the compression of the anterior horn of the spinal cord on both sides, while most of them come from abdominal compression (Figure 2A–C). The axial area of the WT group was larger than that of the model group, and the minimum axial area and diameter of the vertebral canal decreased with increasing age of the *Enpp1flox/flox*/*EIIa-Cre* group but with no statistical significance at 20 to 28 weeks. Similarly, HE/CT measurements of the spinal cord/spinal canal-to-vertebral body ratio showed similar results (Figure S1B). The above results demonstrated a close correlation between CT and histological findings.

3.4 | HE staining and LFB staining of the myelin sheath

HE staining showed clear white and gray matter within the spinal cord in the WT group, whereas the *Enpp1flox/flox*/*EIIa-Cre* group showed anterior bony compression and altered pathological morphology of the spinal cord. The WT group had normal neurons clustered in the anterior and posterior horns of the gray matter (at ×40) with a clear boundary with the white matter and a fine texture. In the *Enpp1flox/flox*/*EIIa-Cre* group, however, the boundary between gray and white matter was blurred; vacuoles were formed around gray matter nuclei, and white matter demyelinated to form cavities (Figure 2D). Luxol fast blue staining showed that the spinal cord axons in the WT group were dense without vacuolization, whereas myelin at the site of white matter injury in front of the spinal cord in the *Enpp1flox/flox*/*EIIa-Cre* group was lost. In addition, the surviving myelin appeared disordered in the transverse and coronal sections, and vacuoles around the compression sites appeared in the *Enpp1flox/flox*/*EIIa-Cre* group (Figure 2E).

3.5 | Changes of nerve cells caused by chronic compression

The formation of myelin requires Myelin Basic Protein (MBP). The myelin cells of the central nervous system (CNS) are called oligodendrocytes, and they can produce the second most abundant protein of the central nervous system, called myelin basic protein. Demyelination is characterized by MBP decomposition. Here, we performed immunofluorescence of Mbp to evaluate the changes in gray matter and white matter in the spinal cord (Figure 3A, B). Compared to WT mice, *Enpp1flox/flox*/*EIIa-Cre* mice had a significantly decreased ratio of Mbp immunofluorescence intensity in gray matter to ventral white matter ($p < 0.001$). Immunofluorescence staining of Mbp axial sections showed that the myelin sheath was regularly distributed in WT mice, while *Enpp1flox/flox*/*EIIa-Cre* mice showed demyelination and disorder in both gray matter and white matter. These data suggested that the reduction in oligodendrocytes is associated with chronic compression of the ventral spinal cord in the present model (Figure 3C, D).

Compared to the WT group, Neun-positive cells in the *Enpp1flox/flox*/*EIIa-Cre* group decreased ($p < 0.05$), and most neurons in the ipsilateral ventral horn were destroyed (Figure 3E, F). Neun-positive areas, mainly in the anterior horn, decreased with spinal cord

FIGURE 2   Age-related spinal canal narrowing and spinal cord compression in mice: Micro-CT and histological correlation. (A) Three-dimensional reconstruction and representative sagittal and axial micro-CT images of the compressive segment. The white arrow indicates the compression site, and the spatial area of the spinal cord in the cross section was gradually reduced. (B, C) The minimum area and the minimum sagittal diameter of the spinal canal in mice decrease with age. Compared with the WT group (28 W), the minimum area and the minimum sagittal diameter of the spinal canal were decreased in *Enpp1flox/flox*/*EIIa-Cre* group (28 W) mice. (D) Calcified lesions originating from vertebral body in *Enpp1flox/flox*/*EIIa-Cre* mice (black arrow heads), compressing the spinal cord segments laterally or posteriorly. (E) LFB staining shows Spotted holes caused by the separation of myelin sheaths from the axons in the anterior columns in *Enpp1flox/flox*/*EIIa-Cre* mice. Note also swelling and deformity of axons particularly in the anterior columns (black arrow heads) in *Enpp1flox/flox*/*EIIa-Cre* mice. Data are expressed as mean ± SD. *$p < 0.05$, **$p < 0.01$, ***$p < 0.001$, ****$p < 0.0001$, scale bar 200 μm.
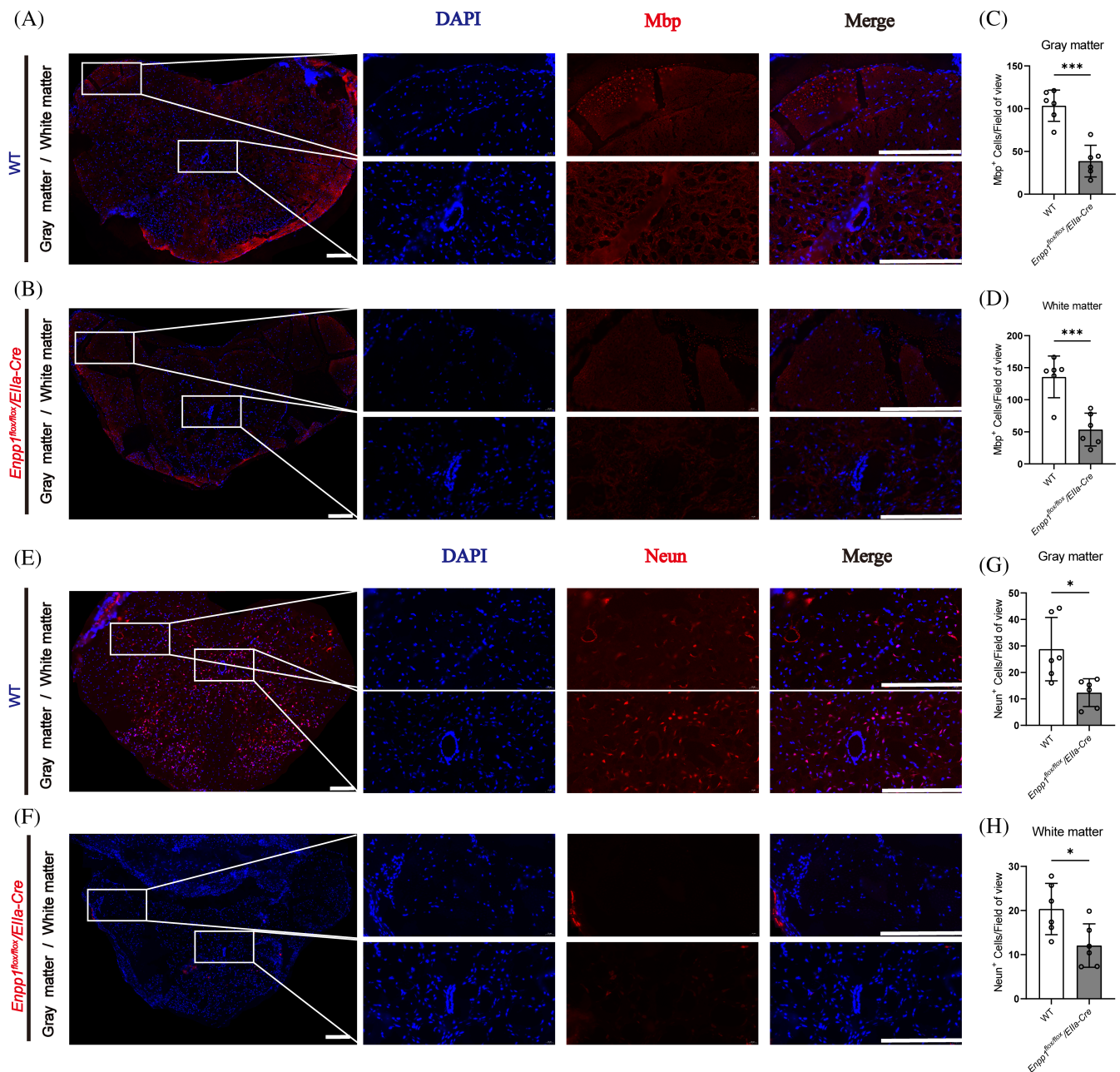
FIGURE 3   White and gray matter damage in *Enpp1*$^{flox/flox}$/*EIIa-Cre* mice with chronic spinal cord compression. (A, B) Mbp immunostaining of spinal cord sections. (E, F) Neun immunostaining of spinal cord sections. (C, D, G, H) Chronic progressive compression of the cervical spinal cord significantly decreased the expression of myelin sheath and neurons, as measured by unbiased cells/fields of view. Data are expressed as mean ± SEM. *$p < 0.05$, **$p < 0.01$, ***$p < 0.001$, ****$p < 0.0001$, *Enpp1*$^{flox/flox}$/*EIIa-Cre* versus WT group ($n = 6$:6). scale bar 200 μm.

compression. These results indicated that one of the major tissue injuries in this model is the loss of ipsilateral gray matter (Figure 3G, H).

Astrocytes can cause CNS inflammation by acquiring immune cell functions, producing cytokines and chemokines to influence effector cells, modulating the blood–brain barrier, and forming the glial scar. The degree of astrogliosis and the severity of SCI were evaluated with anti-GFAP antibodies, and morphometric measurements of Gfap-positive areas were performed using six axial sections. Compared to WT mice, there was a significant increase of astrocytes in both the gray and white matter of WT mice (Figure 4A, B). A marked increase

in Gfap immunofluorescence intensity around the central canal of the spinal cord, representing astrogliosis around the central canal, was observed in the *Enpp1*$^{flox/flox}$/*EIIa-Cre* group (21.50 ± 9.29). Larger Gfap-positive areas (6.21 ± 4.29) were observed in the anterior horn tissue at both ends of the ventral flank of *Enpp1*$^{flox/flox}$/*EIIa-Cre* mice with trabeculae surrounding the injury site and a significant reduction in the area of spared tissue as indicated by Gfap-positive expression (Figure 4C, D).

To evaluate the changes in macrophages/microglia in the chronically compressed cervical spinal cord, we measured the expression of
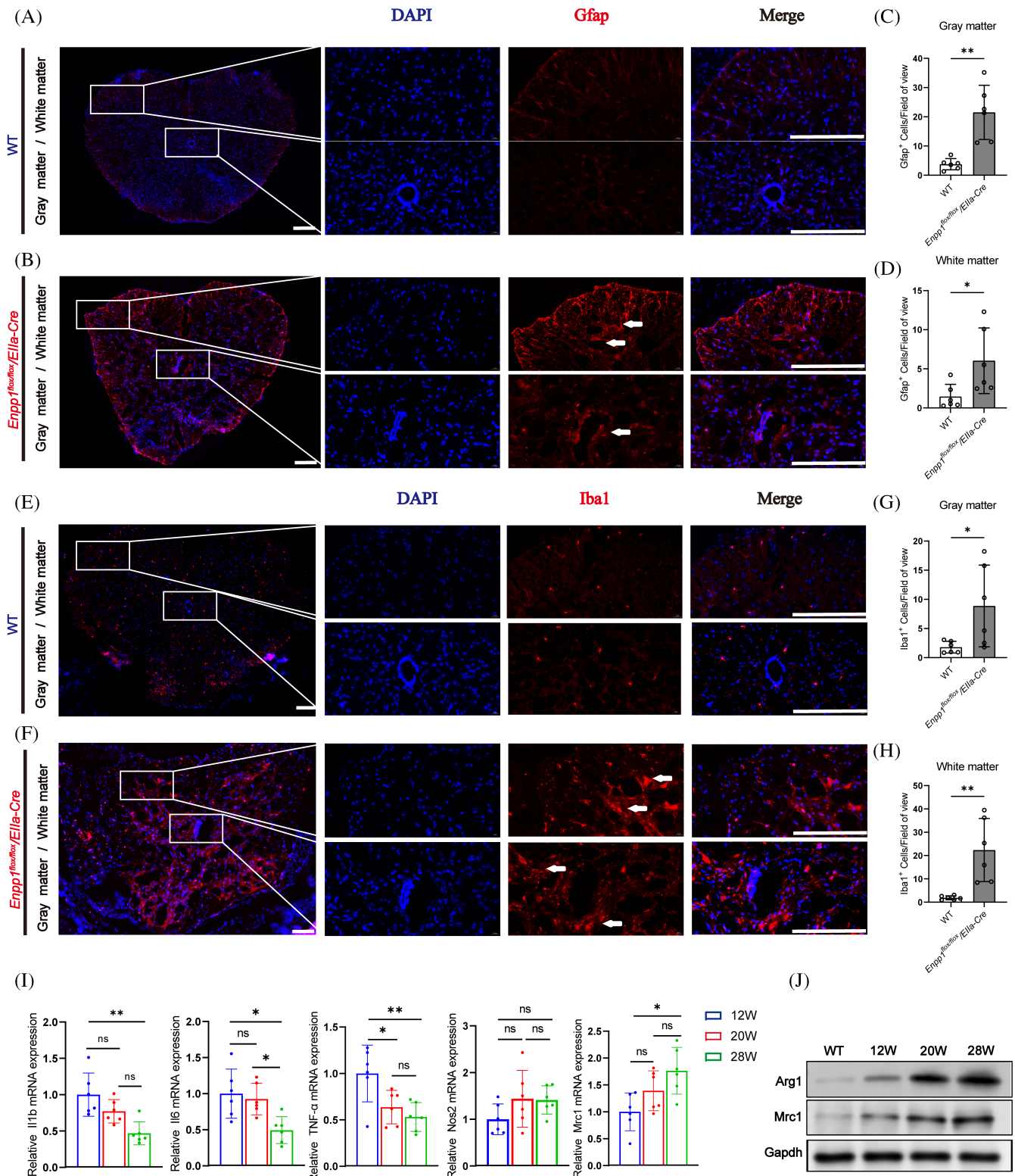
FIGURE 4 Increased inflammation and macrophage activation in *Enpp1*^flox/flox^/*EIIa-Cre* mice: Immunostaining and gene expression analysis. (A, B), E, F) Gfap and Iba1 immunostaining of spinal cord sections. Representative images of immunostaining for WT and *Enpp1*^flox/flox^/*EIIa-Cre* group. The arrow indicates the Gfap, Iba1—positive cells. (C, D), (G, H) *Enpp1*^flox/flox^/*EIIa-Cre* mice showed increased expression of Gfap and Iba1, as measured by unbiased cells/fields of view. (I) Relative Il1b, Il6, TNF-α, Nos2, and Mrc1 expression, as assessed by qRT-PCR. (J) Analysis of Arg1 and Mrc1 protein expression levels. Data are expressed as mean ± SD. *$p < 0.05$, **$p < 0.01$, ***$p < 0.001$, ****$p < 0.0001$, *Enpp1*^flox/flox^/*EIIa-Cre* versus WT group ($n = 6{:}6$). Scale bar 200 μm.
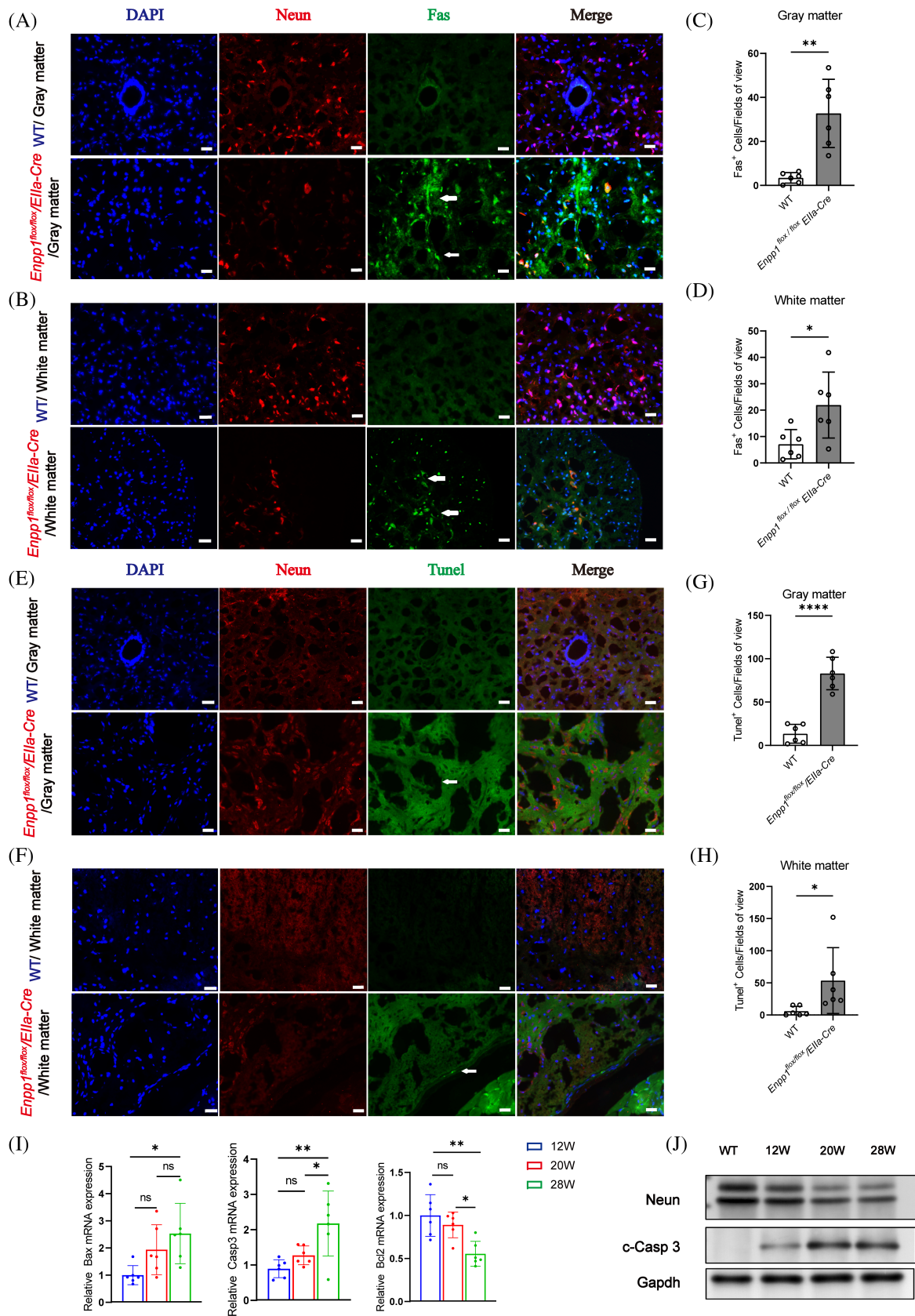
FIGURE 5 Legend on next page.

IBA1 protein in the spinal cord. There was a statistically significant difference in the relative density between the WT group and the *Enpp1^{flox/flox}/EIIa-Cre* group ($p < 0.05$). In the compressed anterior horn of the spinal cord, the Iba1-labeled cells in the *Enpp1^{flox/flox}/EIIa-Cre* group were larger, and rounder compared to those in the WT group, indicating an activated state of macrophages/microglia (Figure 4E, H). Il-1b, Il-6, and Tnf-α expression in the spinal cord were higher at 12 weeks in the *Enpp1^{flox/flox}/EIIa-Cre* group but not significantly different from the 20 to 28 weeks, while the expression levels of Nos2 and Mrc1 increased with increasing age in *Enpp1^{flox/flox}/EIIa-Cre* mice (Figure 4I). At the protein level, the expression levels of Arg1 and Mrc1 show a progressive increase in response to the severity of spinal cord compression. This finding indicates a gradual deterioration of chronic inflammation as the degree of compression worsens (Figure 4J).

3.6 | Neuronal apoptosis in mice with cervical cord compression

The loss of spinal nerve function is caused by neuronal apoptosis, which is a key aspect of OPLL myelopathy. To detect apoptotic degradation, we employed a fluorescence in situ apoptosis detection kit to distinguish between the two groups. Fas immunoreactivity was highly expressed in 32.70 ± 15.50% of neurons on gray matter and in 21.93 ± 12.50% of neurons on white matter in *Enpp1^{flox/flox}/EIIa-Cre* group (Figure 5A–D). In contrast, compared to the WT group, the number of TUNEL-positive cells was significantly increased in the *Enpp1^{flox/flox}/EIIa-Cre* group ($p < 0.0001$). Rare TUNEL-positive neurons were found in the gray and white matter of the spinal cord in control WT mice. In addition, TUNEL-positive cells were found in gray and white matter, especially in the front corner of the *Enpp1^{flox/flox}/EIIa-Cre* group. Quantification of cells double-labeled with Neun and TUNEL showed that many of these apoptotic cells were neurons. Fas expression was found at very low levels in 3.44 ± 2.41% of neurons on gray matter and in 7.10 ± 5.53% of neurons on white matter (Figures 5E–H) in WT mice. In addition, we used RT-qPCR to evaluate the expression levels of Bcl2, Bax, and Caspase 3, which indicated a significant decrease in Bcl2 and the Neun neuronal marker as well as an increase in Bax and Caspase 3 in the *Enpp1^{flox/flox}/EIIa-Cre* group (Figure 5I). At the protein level, the expression of Neun shows a gradual decline from week 12 to 28, while there is a concurrent increase in c-Casp3 expression (Figure 5J).

3.7 | Expression of Vegf and Vwf in the decompressed spinal cord

VEGF and VWF have been reported as angiogenesis markers in many diseases. Recently, many researchers have proposed that axonal degeneration, vascular dysfunction, and neuronal destruction may be the key processes of neural function recovery after decompression. Therefore, we further investigated the expression of Vegf and Vwf in the spinal cord to evaluate the potential effect of chronic compression of the spinal cord by ectopic ossification of the spinal canal on angiogenesis. Compared to the WT group, the expression levels of Vegf in the anterior horn and Vwf in the white matter and gray matter of the spinal cord decreased in the *Enpp1^{flox/flox}/EIIa-Cre* group, and the vascular endothelial cells and accompanying neurons in the spinal cord also decreased in the *Enpp1^{flox/flox}/EIIa-Cre* group (Figure 6A–H). Additionally, the mRNA expression of Mmp2 and Mmp9 increased with age in mice, whereas Vegf, Vwf, and Pecam1 expression increased during early compression but decreased after stabilization of the ossific mass at 20 to 28 weeks (Figure 6I). At the protein level, the expression of Vegf exhibits a progressive decline (Figure 6J).

4 | DISCUSSION

This study created and analyzed a mouse model of bony spinal cord compression, resembling the distribution of OPLL. The findings showed that the compressed spinal cord led to a limping gait and impaired limb function, similar to OPLL in humans. In conclusion, the *Enpp1^{flox/flox}/EIIa-Cre* mouse model represents a well-characterized animal model of chronic spinal cord injury, specifically targeting the ventral spinal cord. This model allows for the investigation of neuronal degeneration, demyelination, neuronal activity, oligodendrocyte reduction, microglia, and astrocyte activation, and macrophage aggregation, all associated with OPLL-induced neuroinflammation. Because the growth cycle of mice is relatively consistent, standardized, and quantitative results can be used. The use of this modeling method will reduce the risk of complications, such as acute spinal cord injury, which may result from surgical operations intended to reduce pain in animals. The present findings revealed secondary pathophysiological changes after chronic compression of the ventral spinal cord, including proliferation and apoptosis of various nerve cells as well as a reduction in angiogenesis markers.

FIGURE 5 Apoptosis related to neurons in rats with chronic cervical cord compression. Representative micrograph of axial sections derived from WT mice and *Enpp1^{flox/flox}/EIIa-Cre*. (A, B) Double immunohistochemistry with anti-Fas (green) and anti-Neun (red) antibodies revealed Fas-positive neurons in the *Enpp1^{flox/flox}/EIIa-Cre* mice spinal cord sections in contrast with normal spinal cord sections on white matter and gray matter; (E, F) Double immunohistochemistry with TUNEL (green) and anti-Neun (red) antibodies revealed TUNEL positive neurons in the *Enpp1^{flox/flox}/EIIa-Cre* mice spinal cord sections in contrast with normal spinal cord sections on white matter and gray matter; (C, D, G, H) Chronic progressive compression of the cervical spinal cord significantly increased neuronal and oligodendrocytic apoptosis, as measured by unbiased cells/fields of view. (I) Relative Bax, Casp3 and Bcl2 expression, as assessed by RT-qPCR. (J) Analysis of Neun and c-Casp3 protein expression levels. Data are expressed as mean ± SEM. *$p < 0.05$, **$p < 0.01$, ***$p < 0.001$, ****$p < 0.0001$, *Enpp1^{flox/flox}/EIIa-Cre* versus WT group ($n = 6:6$). Scale bar 200 μm.
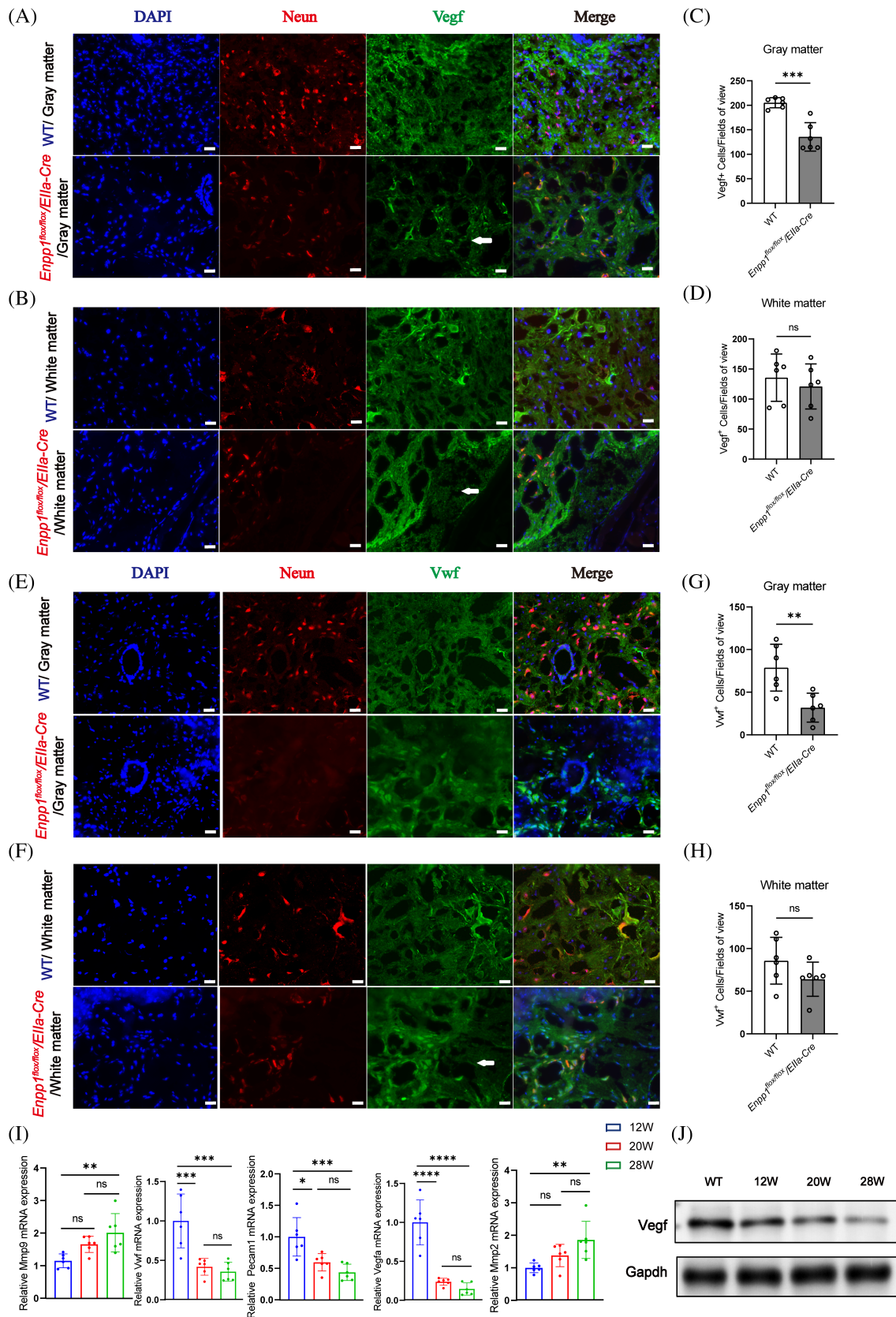
FIGURE 6 Legend on next page.

Myelopathy due to OPLL, which usually results in unstable walking and loss of balance, is the most significant factor affecting the patient's quality of life.[19] Some research groups have described the pathological characteristics of chronic spinal cord compression in OPLL patients, which is similar to the histopathological and pathophysiological changes of traumatic spinal cord injury. The pathological features of the spinal cord of OPLL include degeneration of the central gray matter and white matter as well as degeneration of the corticospinal tract. The compression sites are mostly located at the ventral side and are generally divided into the central type and lateral type in the cross-section. The molecular mechanism of the progressive loss of neurons, oligodendrocytes, and spinal cord demyelination is still uncertain.[20–23] In the present model, the mice were able to care for themselves, including eating, drinking, and grooming, and no urinary retention was observed. Spinal cord injury caused by compression slowly forms and is gradually aggravated. The comparison of the BMS scores provided the most powerful evidence for the difference in the damage of motor neurons in the hind limb and the forelimb. As the mice grew older, the ossification focus gradually increased and compressed the spinal cord nerve, and the spinal cord function score of the mice gradually decreased. The decrease was significant from 12 to 20 weeks, suggesting that the compression of the spinal cord increases with the growth of the ossification block and that the chronic compression of the spinal cord affects the spinal cord nerve function of the mice. The inclined plate test demonstrated that the strength of the mice was also significantly decreased. We further explored the difference between the forelimb and hind limb by analyzing the paw statistics obtained using the catwalk. Most of the parameters showed that the forelimb and hindlimb functions were similar. There was a significant difference in the step length of the forelimb and step width of the hind limb of $Enpp1^{flox/flox}$/EIIa-Cre mice at 12 weeks, and the step length and step width of the forelimb and hind limb were significantly reduced compared to WT mice at 20 weeks. These results align with human findings, as OPLL patients often experience upper limb numbness and loss of fine motor control in their hands.[24–26]

To date, indirect experimental and postmortem pathological studies of patients with cervical spondylosis have revealed necrosis and vacuolization of the gray matter of the spinal cord.[27,28] We also found white matter demyelination cavities in the lesion area in the $Enpp1^{flox/flox}$/EIIa-Cre group with the most severe compression occurring in the ventral anterior horn. Additionally, Luxol fast blue staining and cavitation changes were significantly higher with the spread of spongiform necrosis, and the ventral compression area significantly reduced myelin loss from the injury site. In transverse sections, the surviving myelin sheaths were disorganized. Furthermore, as CT partially correlated with HE staining results and spinal cord compression, it may be used to predict behavioral outcomes.

Immunofluorescence demonstrated that the relative area of Neun-positive cells in the anterior horn decreased in $Enpp1^{flox/flox}$/EIIa-Cre mice, and it was proportional to the degree of spinal cord compression. MBP, a marker of oligodendrocytes, was significantly reduced in both gray matter and the anterior horn in $Enpp1^{flox/flox}$/EIIa-Cre mice. In addition, the $Enpp1^{flox/flox}$/EIIa-Cre group had increased expression of GFAP, an indicator of astrocyte activation, and IBA1, which is present on Iba1-positive macrophages or microglia, in the injury area. Damage to oligodendrocytes and neurons initially occurs at the site of injury. After axonal injury, neurotrophic factors are depleted, resulting in neuronal apoptosis in the region distal to the spinal cord injury. As a result of sustained activation and inflammation of microglia, cytotoxic substances are released, causing pathological responses, such as neuronal necrosis and apoptosis, which negatively impact the ability of tissues to repair themselves postinjury. Activation and polarization of microglia and macrophages were found to be involved in the response to chronic and progressive spinal cord compression. Researchers have previously reported that chronic compression of the twy/twy cervical spinal cord results in the loss of central motor neurons. Furthermore, apoptotic cell death leads to tissue degeneration in chronic compression. In addition, neurological impairment in twy/twy mice is associated with the loss of neurons, oligodendrocytes, demyelination, and reactive astrogliosis.[29–31]

Additionally, compression of the spinal cord by OPLL results in multiple biochemical and pathological events, including hypoxia, ischemia, inflammation, and apoptosis. Based on the present findings, compressive cervical myelopathy is associated with neuronal apoptosis with evidence of Fas-mediated induction of the apoptotic cascade, including activation of caspases 8, 9, and 3. The effector phase of apoptosis involves the activation of both intrinsic and extrinsic pathways of the caspase family. As a result of compression or contusion, the level of Fas in neurons, astrocytes, and oligodendrocytes is significantly increased. Zurita et al. suggested that Fas expression is enhanced in the gray matter of rats following acute traumatic SCI and predominantly in the white matter 8–72 h after injury.[32] The present study indicated that most of the apoptotic cells expressing Fas in ventral chronic persistent spinal cord compression were neuronal cells, which were predominantly located in the anterior horn region of the spinal cord. The spinal cords of $Enpp1^{flox/flox}$/EIIa-Cre mice had increased mRNA expression levels of apoptosis-related genes

FIGURE 6 Angiogenesis-associated neurons in the compressed cord. Representative micrograph of axial sections derived from WT mice and $Enpp1^{flox/flox}$/EIIa-Cre. (A, B) Double immunohistochemistry with anti-Vegf (green) and anti-Neun (red) antibodies revealed Vegf-positive neurons in the $Enpp1^{flox/flox}$/EIIa-Cre mice spinal cord sections in contrast with normal spinal cord sections on white matter and gray matter. (E, F) Double immunohistochemistry with anti-Vwf (green) and anti-Neun (red) antibodies revealed Vwf-positive neurons in the $Enpp1^{flox/flox}$/EIIa-Cre mice spinal cord sections in contrast with normal spinal cord sections on white matter and gray matter. (C, D, G, H) Chronic progressive compression of the cervical spinal cord significantly decreased neuroangiogenesis, as measured by unbiased cells/fields of view. (I) Relative Vegfa, Vwf, Mmp9, Mmp2, and Pecam1 expression, as assessed by RT-qPCR. (J) Analysis of Vegf protein expression levels. Data are expressed as mean ± SD. *$p < 0.05$, **$p < 0.01$, ***$p < 0.001$, ****$p < 0.0001$.

(Caspase 3, Bax) but decrease mRNA expression levels of Bcl2, consistent with the extent of chronic compression and compression-induced neuron loss paralleled motor dysfunction. After SCI, astrocytes exhibit edema, activation, inflammatory responses, and apoptosis, and they release many cytotoxic factors. In addition, the TUNEL results revealed apoptotic neuronal cells within the narrowest area of bony compression. Wang et al. demonstrated that both demyelinating and TUNEL-positive cells were present in the chronically compressed postmortem spinal cord of patients who died of OPLL.[33]

The present study demonstrated that neuronal loss resulting from necrotic and apoptotic mechanisms is associated with the activation of microglia and macrophages that produce proinflammatory cytokines, which may contribute to the demyelination induced by spinal cord compression in *Enpp1^flox/flox*/*EIIa-Cre* mice. As a result of microglial activation, inflammatory cytokines (e.g., TNF-a, IL-1b, and IL-6) are released, negatively affecting microglial function after SCI. According to the present findings, Tnf-a, Il-1b, and Il-6 levels were elevated in the spinal cord of 12-week-old mice. However, the overall effects of activated microglia on CNS recovery remain controversial due to the multiple potential conflicts between their capabilities. IL-1b and Il-6 levels were significantly higher in the early phase of chronic spinal cord compression, whereas 28-week-old mice showed a decrease in inflammatory mediators due to late barrier formation with IL-1b and Il-6 levels not significantly different from those of WT mice. As a phagocytic receptor for bacteria, fungi, and other pathogens, Mrc1 plays an important role in the endocytosis of glycoproteins by macrophages. Mrc1 binds both sulfated and nonsulfated polysaccharide chains. Similarly, Nos2 produces nitric oxide (NO), a messenger molecule with multiple functions throughout the body, and it enhances the synthesis of proinflammatory mediators, such as IL6 and IL8, whose expression increases with the progression of the disease. By releasing inflammatory cytokines, proteases, and free radicals from the CNS injury core, neuroinflammation is associated with the prevention of secondary tissue damage.[34–36] It is possible that these changes represent a response of the spinal cord to compression to maintain neuronal function.[37,38]

Several factors, such as inflammation and ischemia, can cause neuronal loss in the injured spinal cord, and an abundant vascular supply is essential for the recovery of function. The reduction of blood flow to the spinal cord is associated with vascular dysfunction after compression, and vascular dysfunction and angiogenesis may affect myelin damage, glial fibrosis, and necrosis after cervical spinal cord compression.[39,40] In the twy/twy model, Tanabe et al. suggested that Hif-1 is possibly increased, causing neuronal cell death under hypoxic stress, whereas Hif-1 has also been reported to stimulate the transcription and expression of multiple angiogenic genes, thereby alleviating secondary injury from spinal cord injury by improving microcirculation and restoring hypoxia.[40] Cheng et al. showed improved hypoxia in rats following surgical decompression by chronic spinal cord compression, and they also reported improved motor function associated with the improvement in hypoxia. After decompression, angiogenic markers, such as Vegf and Vwf, are also increased.[16] The ischemic hypoxic changes in CSCI, however, have not been extensively investigated. The present study indicated that Vegf, Vwf, and Pecam1 exhibit high levels of expression in *Enpp1^flox/flox*/*EIIa-Cre* mice at 12 weeks but revert to almost normal levels or even lower than normal expression levels by 28 weeks. During the early stages of spinal cord compression, Mmp2 and Mmp9 expression gradually increased, accompanied by an increase in inflammation, and the expression of angiogenic factors increased but decreased once the late-stage compression reached equilibrium. A previous study has reported that oxygen levels may affect the production of Mmp2. Mmp9 is an important component of the biology and pathophysiology of the central nervous system, affecting a wide range of processes, including cell proliferation, cell differentiation, ECM remodeling, vascularization, and cell migration.[41–43] Therefore, the expression of Vegf, Vwf, and Mmps may be important in chronic spinal cord injury. According to these studies, secondary spinal cord damage is associated with these processes in mouse models, including ischemia, angiogenesis, elevated levels of inflammatory markers in the spinal cord, apoptosis, and astrocyte activation. Despite the limitations of the present study, these processes may affect neurological recovery. As a result, future research should focus on the mechanisms by which these proteins interact with each other and how they affect neuronal function.
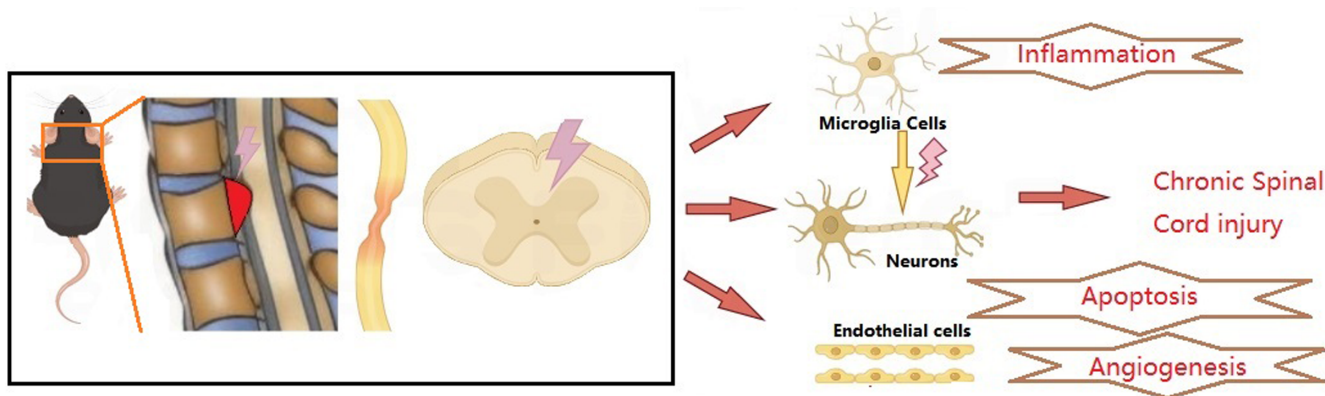

FIGURE 7 Proposed the regulatory mechanism of OPLL induced chronic spinal cord injury.

5 | CONCLUSION

The present study demonstrated that the *Enpp1flox/flox*/*EIIa-Cre* mouse model results in chronic and reproducible spinal cord compression and that the pathological process of spinal cord compression is consistent with mouse behavior and CT findings. The degree of compression is correlated with neurons, oligodendrocyte as well as impaired axonal conduction, neuroinflammatory aggregation, or macrophage accumulation associated with astrocyte and microglial activation. The neurological status of patients may be explained, in part, by the activation of angiogenic factors in the early phase followed by their decreased expression in the late phase. The present model indicated that there is an increase in the expression of inflammatory factors in the spinal cord of mice, which provides some insight into the pathogenesis of OPLL myelopathy (Figure 7). Therefore, we anticipate that the spinal cord compression model will provide new insights into the pathophysiology of OPLL myelopathy and may also be useful in the study of various therapeutic approaches to OPLL.

AUTHOR CONTRIBUTIONS

Zhongyuan He, Tao Tang, Zhengya Zhu and Fuan Wang: conceptualization, methodology, investigation, writing original draft. Jianfeng Li, Fu Zhang, and Nguyen Tran Canh Tung: methodology, data analysis, and figures preparation. Xizhe Liu: conceptualization, supervision, writing, editing, and provided funding support. Zhiyu Zhou: conceptualization, supervision, project administration, and funding acquisition. Shaoyu Liu: conceptualization, resources, supervision, project administration, and funding acquisition. All authors have read and agreed to the published version of the manuscript.

ACKNOWLEDGMENTS

CONFLICT OF INTEREST STATEMENT

The authors declare no conflict of interest.

DATA AVAILABILITY STATEMENT

All data generated or analyzed during this study are available from the corresponding author on reasonable request.

ORCID

Zhongyuan He https://orcid.org/0000-0002-6194-0720
Zhiyu Zhou https://orcid.org/0000-0002-8101-2083

REFERENCES

1. Yoshii T, Yamada T, Hirai T, et al. Dynamic changes in spinal cord compression by cervical ossification of the posterior longitudinal ligament evaluated by kinematic computed tomography myelography. *Spine (Phila Pa 1976)*. 2014;39:113-119.
2. Kawaguchi Y, Urushisaki A, Seki S, Hori T, Asanuma Y, Kimura T. Evaluation of ossification of the posterior longitudinal ligament by three-dimensional computed tomography and magnetic resonance imaging. *Spine J*. 2011;11:927-932.
3. Park S, Lee DH, Ahn J, et al. How does ossification of posterior longitudinal ligament progress in conservatively managed patients. *Spine (Phila Pa 1976)*. 2020;45:234-243.
4. Karadimas SK, Moon ES, Yu WR, et al. A novel experimental model of cervical spondylotic myelopathy (CSM) to facilitate translational research. *Neurobiol Dis*. 2013;54:43-58.
5. Abbaszadeh F, Jorjani M, Joghataei MT, Mehrabi S. Astaxanthin modulates autophagy, apoptosis, and neuronal oxidative stress in a rat model of compression spinal cord injury. *Neurochem Res*. 2022;47:2043-2051.
6. Sun YL, Li G, Zheng Z, et al. A neuronal apoptosis model induced by spinal cord compression in rat. *J Vis Exp*. 2021;29:172.
7. Horak T, Horakova M, Svatkova A, et al. In vivo molecular signatures of cervical spinal cord pathology in degenerative compression. *J Neurotrauma*. 2021;38:2999-3010.
8. Forgione N, Karadimas SK, Foltz WD, Satkunendrarajah K, Lip A, Fehlings MG. Bilateral contusion-compression model of incomplete traumatic cervical spinal cord injury. *J Neurotrauma*. 2014;31:1776-1788.
9. Ma L, Yao Q, Zhang C, Li M, Cheng L, Jian F. Chronic extradural compression of spinal cord leads to syringomyelia in rat model. *Fluids Barriers CNS*. 2020;17:50.
10. Forgione N, Chamankhah M, Fehlings MG. A mouse model of bilateral cervical contusion-compression spinal cord injury. *J Neurotrauma*. 2017;34:1227-1239.
11. Kasahara K, Nakagawa T, Kubota T. Neuronal loss and expression of neurotrophic factors in a model of rat chronic compressive spinal cord injury. *Spine (Phila Pa 1976)*. 2006;31:2059-2066.
12. Yao M, Li G, Pu P, et al. Neuroinflammation and apoptosis after surgery for a rat model of double-level cervical cord compression. *Neurochem Int*. 2022;157:105340.
13. Wang J, Wang X, Rong W, Lv J, Wei F, Liu Z. Alteration in chondroitin sulfate proteoglycan expression at the epicenter of spinal cord is associated with the loss of behavioral function in tiptoe walking Yoshimura mice. *Neurochem Res*. 2014;39:2394-2406.
14. Kim P, Haisa T, Kawamoto T, Kirino T, Wakai S. Delayed myelopathy induced by chronic compression in the rat spinal cord. *Ann Neurol*. 2004;55:503-511.
15. Poon PC, Gupta D, Shoichet MS, Tator CH. Clip compression model is useful for thoracic spinal cord injuries: histologic and functional correlates. *Spine (Phila Pa 1976)*. 2007;32:2853-2859.
16. Cheng X, Yu Z, Xu J, Quan D, Long H. Pathophysiological changes and the role of Notch-1 activation after decompression in a compressive spinal cord injury rat model. *Front Neurosci*. 2021;15:579431.
17. Basso DM, Fisher LC, Anderson AJ, Jakeman LB, Mctigue DM, Popovich PG. Basso mouse scale for locomotion detects differences in recovery after spinal cord injury in five common mouse strains. *J Neurotrauma*. 2006;23:635-659.
18. de Medinaceli L, Church AC, Wang YN. Posttraumatic autoimmune reaction in peripheral nerve: effect of two successive injuries at different locations. *Exp Neurol*. 1985;88:396-404.

19. Machino M, Ando K, Kobayashi K, et al. Alterations in intramedullary T2-weighted increased signal intensity following laminoplasty in cervical spondylotic myelopathy patients: comparison between pre- and postoperative magnetic resonance images. *Spine (Phila Pa 1976)*. 2018;43:1595-1601.

20. Wei L, Cao P, Xu C, et al. The relationship between preoperative factors and the presence of intramedullary increased signal intensity on T2-weighted magnetic resonance imaging in patients with cervical spondylotic myelopathy. *Clin Neurol Neurosurg*. 2019;178:1-6.

21. Matsunaga S, Sakou T, Taketomi E, Komiya S. Clinical course of patients with ossification of the posterior longitudinal ligament: a minimum 10-year cohort study. *J Neurosurg*. 2004;100:245-248.

22. Matsunaga S, Nakamura K, Seichi A, et al. Radiographic predictors for the development of myelopathy in patients with ossification of the posterior longitudinal ligament: a multicenter cohort study. *Spine (Phila Pa 1976)*. 2008;33:2648-2650.

23. Fujiyoshi T, Yamazaki M, Okawa A, et al. Static versus dynamic factors for the development of myelopathy in patients with cervical ossification of the posterior longitudinal ligament. *J Clin Neurosci*. 2010; 17:320-324.

24. Koyanagi I. Options of management of the patient with mild degenerative cervical myelopathy. *Neurosurg Clin N Am*. 2018;29:139-144.

25. Kim B, Yoon DH, Shin HC, et al. Surgical outcome and prognostic factors of anterior decompression and fusion for cervical compressive myelopathy due to ossification of the posterior longitudinal ligament. *Spine J*. 2015;15:875-884.

26. Fujimori T, Le H, Ziewacz JE, et al. Is there a difference in range of motion, neck pain, and outcomes in patients with ossification of posterior longitudinal ligament versus those with cervical spondylosis, treated with plated laminoplasty? *Neurosurg Focus*. 2013;35:E9.

27. Anjum A, Yazid MD, Fauzi Daud M, et al. Spinal cord injury: pathophysiology, multimolecular interactions, and underlying recovery mechanisms. *Int J Mol Sci*. 2020;21:21.

28. Bhattacharyya S. Spinal cord disorders: myelopathy. *Am J Med*. 2018; 131:1293-1297.

29. Ichikawa N, Kumagai G, Wada K, et al. Coagulation, vascular morphology, and vasculogenesis in spinal ligament ossification model mice. *Spine (Phila Pa 1976)*. 2021;46:E802-E809.

30. Takeura N, Nakajima H, Watanabe S, Honjoh K, Takahashi A, Matsumine A. Role of macrophages and activated microglia in neuropathic pain associated with chronic progressive spinal cord compression. *Sci Rep*. 2019;9:15656.

31. Hirai T, Uchida K, Nakajima H, et al. The prevalence and phenotype of activated microglia/macrophages within the spinal cord of the hyperostotic mouse (twy/twy) changes in response to chronic progressive spinal cord compression: implications for human cervical compressive myelopathy. *PLoS One*. 2013;8:e64528.

32. Zurita M, Vaquero J, Zurita I. Presence and significance of CD-95 (Fas/APO1) expression after spinal cord injury. *J Neurosurg*. 2001;94: 257-264.

33. Yamaura I, Yone K, Nakahara S, et al. Mechanism of destructive pathologic changes in the spinal cord under chronic mechanical compression. *Spine (Phila Pa 1976)*. 2002;27:21-26.

34. Niehaus JK, Taylor-Blake B, Loo L, Simon JM, Zylka MJ. Spinal macrophages resolve nociceptive hypersensitivity after peripheral injury. *Neuron*. 2021;109:1274-1282.e1276.

35. Kobashi S, Terashima T, Katagi M, et al. Transplantation of M2-deviated microglia promotes recovery of motor function after spinal cord injury in mice. *Mol Ther*. 2020;28:254-265.

36. Stewart AN, Lowe JL, Glaser EP, et al. Acute inflammatory profiles differ with sex and age after spinal cord injury. *J Neuroinflammation*. 2021;18:113.

37. Ellman DG, Lund MC, Nissen M, et al. Conditional ablation of myeloid TNF improves functional outcome and decreases lesion size after spinal cord injury in mice. *Cells*. 2020;9:2407.

38. Ellman DG, Degn M, Lund MC, et al. Genetic ablation of soluble TNF does not affect lesion size and functional recovery after moderate spinal cord injury in mice. *Mediators Inflamm*. 2016;2016:2684098.

39. Zhou Y, Liu XH, Qu SD, et al. Hyperbaric oxygen intervention on expression of hypoxia-inducible factor-1α and vascular endothelial growth factor in spinal cord injury models in rats. *Chin Med J (Engl)*. 2013;126:3897-3903.

40. Hu R, Shi M, Xu H, et al. Integrated bioinformatics analysis identifies the effects of Sema3A/NRP1 signaling in oligodendrocytes after spinal cord injury in rats. *PeerJ*. 2022;10:e13856.

41. Jiang S, Wu Y, Wu S, et al. Silencing TAK1 reduces MAPKs-MMP2/9 expression to reduce inflammation-driven neurohistological disruption post spinal cord injury. *Cell Death Discov*. 2021;7:96.

42. Lee JY, Na WH, Choi HY, Lee KH, Ju BG, Yune TY. Jmjd3 mediates blood-spinal cord barrier disruption after spinal cord injury by regulating MMP-3 and MMP-9 expressions. *Neurobiol Dis*. 2016;95: 66-81.

43. Zhang C, Li D, Hu H, et al. Engineered extracellular vesicles derived from primary M2 macrophages with anti-inflammatory and neuroprotective properties for the treatment of spinal cord injury. *J Nanobiotechnol*. 2021;19:373.

SUPPORTING INFORMATION

Additional supporting information can be found online in the Supporting Information section at the end of this article.